Reconfigurability analysis of multirotor UAVs

Marco Maccotta and Marco Lovera

Abstract The most common fault type for multirotors is the loss of one of the propulsive units (because of aerodynamic, mechanical or electrical issues). To face such a fault one must reconfigure the multirotor so that balance of vertical forces and momenta about the three axes can still be guaranteed with the remaining units. In this paper the approach proposed in[1] is applied to multirotor configurations under study for the design of a multirotor platform for inspections in oil & gas plants. More specifically two classes of multirotors are studied: first hexacopters with H configuration are considered; subsequently octocopters are studied.

1 Introduction

Multirotor UAVs are becoming increasingly popular for civil applications. Their more and more widespread use, however, increases the relevance of fault analysis and fault management, with specific reference to attitude control systems. The problem has been studied extensively in the literature (see, *e.g.*, the survey paper[2]) and a number of approaches to fault detection and reconfiguration specific for multirotors have been proposed. For multirotors the most common fault is the loss of one of the propulsive units (because of aerodynamic, mechanical or electrical issues). To face such a fault one must reconfigure the multirotor so that balance of vertical forces and momenta about the three axes can still be guaranteed with the remaining units. The problem of reconfigurability analysis therefore is of great significance. Among others, the method proposed in[1] is particularly appealing as it relies solely on structural information and in the case of multirotors allows to conclude on re-

Marco Maccotta
Politecnico di Milano, e-mail: marco.maccotta@mail.polimi.it

Marco Lovera
Politecnico di Milano, e-mail: marco.lovera@polimi.it

configurability in terms of the so-called *mixer matrix*, which is an integral part of most attitude control implementations for multirotors. In the cited paper structural reconfigurability is studied for conventional hexacopters. In the present paper, on the other hand, different configurations are considered, as part of a more general study aimed at the design of a multirotor platform for inspections in oil & gas plants. More specifically two classes of multirotors are studied: first hexacopters with H configuration are considered; subsequently octocopters are studied. The results show that the hexacopters are not fully reconfigurable, while the octocopters are, even though the specific choice for the assignment of signs of rotation to the individual rotors affects the achievable performance.

2 Reconfigurability analysis

Fault tolerant control (FTC) is the branch of control engineering which aims at solving the problem of automatically handing the effect of faults or failures through a process of diagnosis, isolation and reconfiguration. The diagnosis unit has the task of detecting the occurrence of a fault, while the isolation unit deals with the problem of characterising the specific fault f. Once a fault has been isolated three possible situations may arise:

- If the fault is negligible, then a redesign the existing control system may be avoided, as long as it is endowed with an appropriate robustness level (this case is usually referred to as passive fault tolerance);
- If the fault is significant but not too critical, then it is possible to modify the controller parameters without modifying its structure (so-called active fault tolerance, possibly via the use of adaptive systems);
- Finally, if the fault is critical, such as, *e.g.*, in the case of loss of sensors or actuators, it is necessary to reconfigure the system (active fault tolerance).

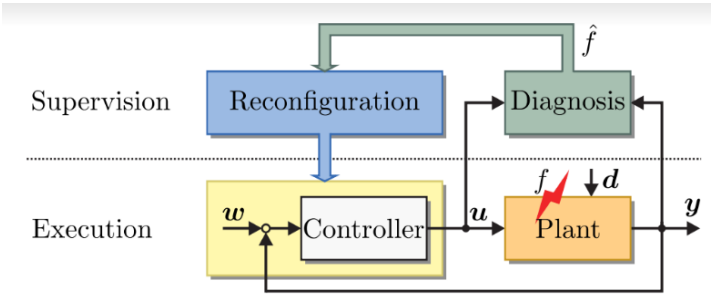

Fig. 1. Active fault control scheme (from [1])

The block diagram in Figure 1 presents an active FTC scheme. The diagnoser isolates the fault and then a reconfiguration unit adapts the controller. Whether a system can be reconfigured or not depends on the physical structure and the presence of redundancies. The availability of such redundancy is the purpose of a reconfigurability analysis. In this work the consequences of a complete loss of a rotor are analysed. The desired flight condition which has to be recovered after a rotor failure is hovering flight. The reconfiguration is performed by using a Linear Virtual Actuator (LVA). Given a linear time-invariant (LTI) system:

$$\dot{x} = Ax + Bu \quad x(0) = x_0 \tag{1}$$

$$y = Cx \tag{2}$$

where the state is denoted by $x \in \mathbb{R}^n$, the input by $u \in \mathbb{R}^m$ and the output $y \in \mathbb{R}^r$; the actuator failure is modelled by the faulty plant:

$$\dot{x_f} = Ax_f + B_f u_f \quad x(0) = x_0 \tag{3}$$

$$y_f = Cx_f, \tag{4}$$

where B_f is the faulty input matrix obtained from B by setting to zero the column corresponding to the failed actuator. In order to be able to use a LVA, *i.e.*,

$$u_f = Nu, \quad N = B_f^+ B, \tag{5}$$

it must be proved that $rank(B_F) = rank(B_f B)$ with $B_f N = B$.

The reconfigurability of a LTI system can be studied through structure matrices and diagraphs. More precisely, the structure matrix of a matrix M can be obtained marking all non zero elements with the '*'-symbol, every zero element as zero. In this way it is possible to compute the structual rank, marking all non-zero elements in different rows and columns by $\circledast$. For example

$$M = \begin{bmatrix} 1 & 2 \\ 0 & 4 \end{bmatrix} \Longrightarrow s\text{-}rank(S_M) = \begin{bmatrix} \circledast & * \\ 0 & \circledast \end{bmatrix}. \tag{6}$$

A digraph on the other hand consists of a set of directed edges ε and a set of vertices v. An edge is an ordered pair of vertices (v_j, v_k). A path is a set of one or more successive edges. Therefore, a path is said to be input-connected if there exists a path from at least one input vertex to every state vertex.

A structural model (given by structure matrices), defines a class of systems. In other words, all the systems that have the same structure belong to the same class. A class is described by matrices S_A, S_B, S_C. As shown in [1], structural matrices and digraphs can be used to test the null-controllability of UAVs which is required to recover hovering flight in case of rotor failure.

3 Multirotor model

A simplified model of the dynamics of the multirotor in near hovering conditions will be used. has been computed in order to be able to design a linear controller. Considering as starte variables the conventional flight dynamics states

$$x = \begin{bmatrix} N\ E\ D\ u\ v\ w\ p\ q\ r \\ \Phi\ \Theta\ \Psi \end{bmatrix}^T, \tag{7}$$

when the system is linearised around the equilibrium point $\bar{x}$ corresponding to hover, with:

$$\bar{x} = \begin{bmatrix} \bar{N}\ \bar{E}\ \bar{D}\ 0_{1\times 9} \end{bmatrix}^T \tag{8}$$

$$\delta x = x - \bar{x} \tag{9}$$

$$\delta u = \begin{bmatrix} \delta F_z\ \delta L\ \delta M\ \delta N \end{bmatrix}^T \tag{10}$$

then the linearised model can be written as a function of the rotor speeds (see also[3]) $u_i(t) = \Omega_i(t)^2$as:

$$\delta\dot{x}(t) = A\delta x(t) + \begin{bmatrix} 0_{5\times N_r} \\ \tilde{B} \\ 0_{3\times N_r} \end{bmatrix} \delta u(t) \tag{11}$$

where the state vector $\delta x(t)$ is defined in (10) and matrix $A \in \mathbb{R}^{n\times n}$ can be obtained from the state equations. The input vector $\delta u(t) \in \mathbb{R}^{N_r}$ contains the N_r variables $\delta u_i(t) = \Omega_i(t)^2 - \bar{\Omega}_i^2$, where $\bar{\Omega}_i = \sqrt{\frac{mg}{K_T N_r}}$ and N_r is the number of rotors. Finally, $\tilde{B}$ is given by

$$\tilde{B} = J^{-1}\chi, \tag{12}$$

i.e., it coincides with the so called *mixer matrix* χ of the motors, which relates forces and moments with rotational speeds, multiplied by the diagonal matrix J^{-1}:

$$J^{-1} = \begin{bmatrix} 1/m & 0 & 0 & 0 \\ 0 & 1/I_{xx} & 0 & 0 \\ 0 & 0 & 1/I_{yy} & 0 \\ 0 & 0 & 0 & 1/I_{zz} \end{bmatrix}. \tag{13}$$

Note that the mixer matrix strictly depends on the structure of the unmanned aerial vehicle and on the rotors rotation direction (clockwise or counter-clockwise). Therefore, (as described in[1]) matrix $\tilde{B}$ is taken into account to analyse the reconfigurability of multirotors.

4 Considered configurations

In this paper two hexarotors (Figures 2a and 2b and mixer matrices (18), (19) respectively) and two octorotors configurations (Figures 3a and 3b and mixer matrices (20), (21) respectively) have been considered.

4.1 External forces and moments

In order to define the forces and moments, the multicopter geometry has to be considered. Starting from the hexarotor, two configurations have been taken into account depending on the direction of rotation of the propellers.

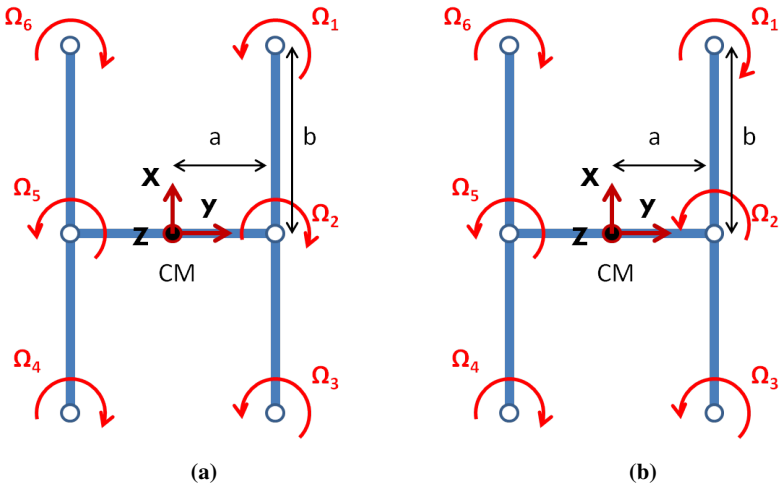

Fig. 2. (a) H_1 (PNPNPN) configuration; (b) H_2 (NPPNPN) configuration.

Naming with **P** the propellers whose rotation causes a positive yaw motion and with **N** those which cause a negative yaw motion, in Figures 2a and 2b the chosen configurations, the label of each propeller, and its rotation direction are pictured. Concerning forces and moments, it is assumed that each propeller produces a thrust T and a torque Q proportional to the square of the angular rate ($T = K_T\Omega^2$, $Q = K_Q\Omega^2$).

Then in the case of the hexacopters forces and moments produced by the six propellers for the PNPNPN configuration, are:

$$F_{prop} = -\begin{bmatrix} 0 \\ 0 \\ K_T(\Omega_1^2+\Omega_2^2+\Omega_3^2+\Omega_4^2+\Omega_5^2+\Omega_6^2) \end{bmatrix} \tag{14}$$

$$M_{prop} = \begin{bmatrix} L \\ M \\ N \end{bmatrix} = \begin{bmatrix} K_T a(-\Omega_1^2 - \Omega_2^2 - \Omega_3^2 + \Omega_4^2 + \Omega_5^2 + \Omega_6^2) \\ K_T b(\Omega_1^2 - \Omega_3^2 - \Omega_4^2 + \Omega_6^2) \\ K_Q(\Omega_1^2 - \Omega_2^2 + \Omega_3^2 - \Omega_4^2 + \Omega_5^2 - \Omega_6^2) \end{bmatrix} \tag{15}$$

and for the NNPNPN configuration:

$$F_{prop} = -\begin{bmatrix} 0 \\ 0 \\ K_T(\Omega_1^2 + \Omega_2^2 + \Omega_3^2 + \Omega_4^2 + \Omega_5^2 + \Omega_6^2) \end{bmatrix}, \tag{16}$$

$$M_{prop} = \begin{bmatrix} L \\ M \\ N \end{bmatrix} = \begin{bmatrix} K_T a(-\Omega_1^2 - \Omega_2^2 - \Omega_3^2 + \Omega_4^2 + \Omega_5^2 + \Omega_6^2) \\ K_T b(\Omega_1^2 - \Omega_3^2 - \Omega_4^2 + \Omega_6^2) \\ K_Q(-\Omega_1^2 + \Omega_2^2 + \Omega_3^2 - \Omega_4^2 + \Omega_5^2 - \Omega_6^2) \end{bmatrix}. \tag{17}$$

Forces and moments can be rearranged to realize the mixer matrix χ of the motors, which relates forces and moments with rotational speeds. Therefore, marking as χ_{H_1} and χ_{H_2} the mixer matrices for the PNPNPN and the NPPNPN configuration, respectively, we have:

$$\chi_{H_1} = \begin{bmatrix} -K_T & -K_T & -K_T & -K_T & -K_T & -K_T \\ -K_T a & -K_T a & -K_T a & K_T a & K_T a & K_T a \\ K_T b & 0 & -K_T b & -K_T b & 0 & K_T b \\ K_Q & -K_Q & K_Q & -K_Q & K_Q & -K_Q \end{bmatrix}, \tag{18}$$

$$\chi_{H_2} = \begin{bmatrix} -K_T & -K_T & -K_T & -K_T & -K_T & -K_T \\ -K_T a & -K_T a & -K_T a & K_T a & K_T a & K_T a \\ K_T b & 0 & -K_T b & -K_T b & 0 & K_T b \\ -K_Q & K_Q & K_Q & -K_Q & K_Q & -K_Q \end{bmatrix}. \tag{19}$$

Similarly, for the octocopters (see again the configurations in Figure 3), the mixer matrices have been computed as:

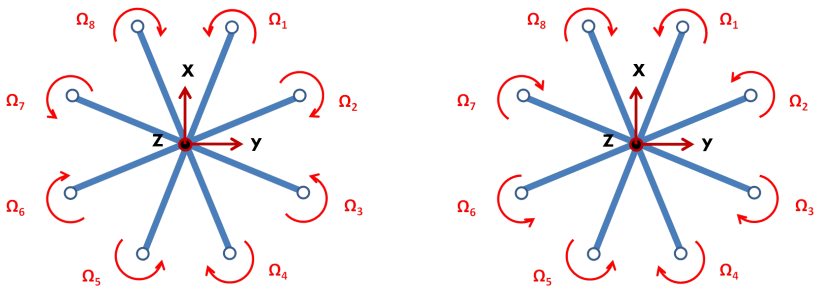

Fig. 3. (a) PNPNPNPN configuration; (b) PPNNPPNN configuration.

$$\chi_{O_1} = \begin{bmatrix} -K_T & -K_T & -K_T & -K_T & -K_T & -K_T & -K_T & -K_T \\ -K_T a_{\frac{3\pi}{8}} & -K_T a_{\frac{\pi}{8}} & -K_T a_{\frac{\pi}{8}} & -K_T a_{\frac{3\pi}{8}} & K_T a_{\frac{3\pi}{8}} & K_T a_{\frac{\pi}{8}} & K_T a_{\frac{\pi}{8}} & K_T a_{\frac{3\pi}{8}} \\ K_T b_{\frac{3\pi}{8}} & K_T b_{\frac{\pi}{8}} & -K_T b_{\frac{\pi}{8}} & -K_T b_{\frac{3\pi}{8}} & -K_T b_{\frac{3\pi}{8}} & -K_T b_{\frac{\pi}{8}} & K_T b_{\frac{\pi}{8}} & K_T b_{\frac{3\pi}{8}} \\ K_Q & -K_Q & K_Q & -K_Q & K_Q & -K_Q & K_Q & K_Q \end{bmatrix} \tag{20}$$

$$\chi_{O_2} = \begin{bmatrix} -K_T & -K_T & -K_T & -K_T & -K_T & -K_T & -K_T & -K_T \\ -K_T a_{\frac{3\pi}{8}} & -K_T a_{\frac{\pi}{8}} & -K_T a_{\frac{\pi}{8}} & -K_T a_{\frac{3\pi}{8}} & K_T a_{\frac{3\pi}{8}} & K_T a_{\frac{\pi}{8}} & K_T a_{\frac{\pi}{8}} & K_T a_{\frac{3\pi}{8}} \\ K_T b_{\frac{3\pi}{8}} & K_T b_{\frac{\pi}{8}} & -K_T b_{\frac{\pi}{8}} & -K_T b_{\frac{3\pi}{8}} & -K_T b_{\frac{3\pi}{8}} & -K_T b_{\frac{\pi}{8}} & K_T b_{\frac{\pi}{8}} & K_T b_{\frac{3\pi}{8}} \\ K_Q & K_Q & -K_Q & -K_Q & K_Q & K_Q & -K_Q & -K_Q \end{bmatrix}; \tag{21}$$

where:

$$\begin{aligned} a_{\frac{3\pi}{8}} &= \frac{l}{2}\cos(\frac{3\pi}{8}); \\ a_{\frac{\pi}{8}} &= \frac{l}{2}\cos(\frac{\pi}{8}); \\ b_{\frac{3\pi}{8}} &= \frac{l}{2}\sin(\frac{3\pi}{8}); \\ b_{\frac{\pi}{8}} &= \frac{l}{2}\sin(\frac{\pi}{8}); \end{aligned} \tag{22}$$

with χ_{O_1} and χ_{O_2} the mixer matrices for the PNPNPNPN and the PPNNPPNN configuration respectively; $l/2$ the arm length and $\pi/4$ the angular distance between two consecutive arms.

5 Hexacopter

The application of the reconfigurability analysis is fully described for the H_1 (PNPNPN) hexacopter configuration, with mixer matrix χ_{H_1}. For the sake of conciseness only the results will be presented for configuration H_2.

5.1 Configuration H_1

Renaming as $\tilde{B} = B_{H_1} = J^{-1}\chi_{H_1}$, the result is:

$$B_{H_1} = \begin{bmatrix} -\frac{K_T}{m} & -\frac{K_T}{m} & -\frac{K_T}{m} & -\frac{K_T}{m} & -\frac{K_T}{m} & -\frac{K_T}{m} \\ -\frac{K_T a}{I_{xx}} & -\frac{K_T a}{I_{xx}} & -\frac{K_T a}{I_{xx}} & \frac{K_T a}{I_{yy}} & \frac{K_T a}{I_{xx}} & \frac{K_T a}{I_{xx}} \\ \frac{K_T b}{I_{yy}} & 0 & -\frac{K_T b}{I_{yy}} & -\frac{K_T b}{I_{yy}} & 0 & \frac{K_T b}{I_{yy}} \\ \frac{K_Q}{I_{zz}} & -\frac{K_Q}{I_{zz}} & \frac{K_Q}{I_{zz}} & -\frac{K_Q}{I_{zz}} & \frac{K_Q}{I_{zz}} & -\frac{K_Q}{I_{zz}} \end{bmatrix}, \tag{23}$$

which can be rewritten in a more compact form as

$$B_{H_1} = \begin{bmatrix} -K_z & -K_z & -K_z & -K_z & -K_z & -K_z \\ -K_r a & -K_r a & -K_r a & K_r a & K_r a & K_r a \\ K_p b & 0 & -K_p b & -K_p b & 0 & K_p b \\ K_y & -K_y & K_y & -K_y & K_y & -K_y \end{bmatrix} \tag{24}$$

with $K_z = \frac{K_T}{m}$, $K_r = \frac{K_T}{I_{xx}}$, $K_p = \frac{K_T}{I_{yy}}$ and $K_y = \frac{K_Q}{I_{zz}}$.
Matrix B_{H_1} multiplies the input vector

$$\delta u(t) = \left[\delta u_1(t)\ \delta u_2(t)\ \delta u_3(t)\ \delta u_4(t)\ \delta u_5(t)\ \delta u_6(t)\right]^T, \tag{25}$$

therefore, in the operating point it must hold that $B\delta\bar{u} = 0_{4\times 1}$; which means that:

$$\begin{cases} \sum_{i=1}^{6} -K_T \bar{u}_i = -mg \\ -K_r a\bar{u}_1 - K_r a\bar{u}_2 - K_r a\bar{u}_3 + K_r a\bar{u}_4 + K_r a\bar{u}_5 + K_r a\bar{u}_6 = 0 \\ K_p b\bar{u}_1 - K_p b\bar{u}_3 - K_p b\bar{u}_4 + K_p b\bar{u}_6 = 0 \\ K_y\bar{u}_1 - K_y\bar{u}_2 + K_y\bar{u}_3 - K_y\bar{u}_4 + K_y\bar{u}_5 - K_y\bar{u}_6 = 0. \end{cases} \tag{26}$$

As performed in [1] matrix B_{H_1} is reduced row by row (applying a Gaussian elimination algorithm on the last three rows). The result is a reduced matrix V such that the new virtual input vector is $\delta v(t) = V\delta u(t)$. Then a 4×4 matrix ${B^v}_{H_1}$ is computed to ensure $B_{H_1} = {B^v}_{H_1} V$. This solution allows to find a minimal form of the relations between $\delta v(t)$ and $\delta u(t)$ and to simplify the system reconfigurability analysis. For B_{H_1}, the virtual inputs are given by:

$$\begin{cases} \delta v_1(t) = \sum_{i=1}^{6} \delta u_i(t) \\ \delta v_2(t) = \delta u_1(t) - \delta u_4(t) \\ \delta v_3(t) = \delta u_2(t) - \delta u_5(t) \\ \delta v_4(t) = \delta u_3(t) - \delta u_6(t) \end{cases} \tag{27}$$

which can be also written as:

$$\begin{cases} \delta v_1(t) = v_1(t) - \bar{v}_1 = \sum_{i=1}^{6} u_i(t) - \frac{mg}{K_T} \\ \delta v_2(t) = v_2(t) - \bar{v}_2 = u_1(t) - u_4(t) \\ \delta v_3(t) = v_3(t) - \bar{v}_3 = u_2(t) - u_5(t) \\ \delta v_4(t) = v_4(t) - \bar{v}_4 = u_3(t) - u_6(t). \end{cases} \tag{28}$$

Notice that $\bar{v}_1 = \frac{mg}{K_T}$ while $\bar{v}_i = 0$ for $i = 2, 3, 4$. Then the new matrix ${B^v}_{H_1}$ is:

$$ {B^v}_{H_1} = \begin{bmatrix} -K_z & 0 & 0 & 0 \\ 0 & -K_r a & -K_r a & -K_r a \\ 0 & K_p b & 0 & -K_p b \\ 0 & K_y & -K_y & K_y \end{bmatrix}. \tag{29} $$

Moreover in the operating point we have that

$$ \begin{cases} \bar{v}_1 = \sum_{i=1}^{6} \bar{u}_i = \frac{mg}{K_T} \\ \bar{v}_2 = \bar{u}_1 - \bar{u}_4 = 0 \\ \bar{v}_3 = \bar{u}_2 - \bar{u}_5 = 0 \\ \bar{v}_4 = \bar{u}_3 - \bar{u}_6 = 0. \end{cases} \tag{30} $$

The virtual inputs and the reduced matrix ${B^v}_{H_1}$ are used to test the reconfigurability of the faulty system (proof in[1]). In particular, if after that acuator j fails ($u_j(t) = 0$ and $\bar{u}_j = 0$), there exist virtual faulty inputs $\delta v_{if}(t)$ that are constrained by zero on one side, the column of ${B^v}_{H_1}$ related to this faulty virtual input must be set to zero. The resulting matrix is ${B^v}_{f_{H_1}}$.

Therefore, reconfigurability to a rotor failure of a multirotor UAV can be verified by the following steps:

1. Testing the system input-connectivity through the use of its digraph
2. Testing the reduced rank condition $rank({B^v}_{f_{H_1}}) = rank({B^v}_{H_1}) = 4$.

Notice that, since ${B^v}_{H_1}$ is a square four by four matrix, as soon as one of the virtual inputs $\delta v_{if}(t)$ becomes constrained by zero on one side (because of a motor fault), the UAV becomes non-reconfigurable.

As an example, suppose that motor 1 of the hexacopter H_1 fails; then conditions 1) and 2) have to be checked. The digraph of H_1 is pictured in Figure 4. If motor one ($u_1(t) = 0$) breaks down the digraph remains input connected. Hence, input connectivity is always verified. As the number of rotors increases the number of redundancies raises and requirement 1) remains satisfied. Henceforward, the focus will be pointed on the virtual input matrix.

Condition 2) has to be verified analyzing the virtual inputs $\delta v_i(t)$, $i = 1,..4$. At equilibrium:

$$ \begin{cases} \bar{v}_1 = \sum_{i=1}^{6} \bar{u}_i = \frac{mg}{K_T} \\ \bar{v}_2 = \bar{u}_1 - \bar{u}_4 = 0 \\ \bar{v}_3 = \bar{u}_2 - \bar{u}_5 = 0 \\ \bar{v}_4 = \bar{u}_3 - \bar{u}_6 = 0 \end{cases} \implies \bar{v}_2 = -\bar{u}_4 = 0 \tag{31} $$

while outside the equilibrium:

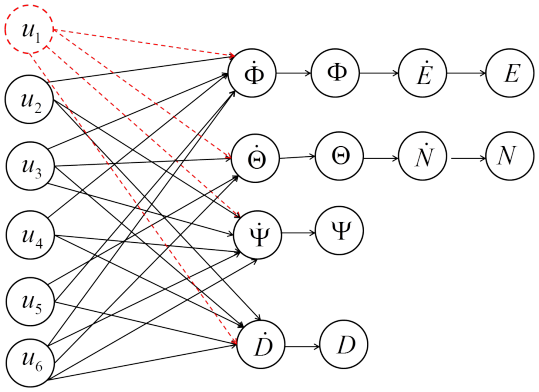

Fig. 4. Digraph of a hexarotor

$$\begin{cases} \delta v_1(t) = \sum_{i=2}^{6} \delta u_i(t) \\ \delta v_2(t) = v_2(t) = -u_4(t) \leq 0 \\ \delta v_3(t) = v_3(t) = u_2(t) - u_5(t) \\ \delta v_4(t) = v_4(t) = u_3(t) - u_6(t). \end{cases} \tag{32}$$

Therefore, the second column of ${B^v}_{H_1}$ must be set to zero and the resulting faulty virtual input matrix $B^v_{f_{H_1}}$ will have rank equal to three. The system is not reconfigurable to a failure on motor 1.

It has been proved that the LVA would not be able to reconfigure the rotors of configuration H_1 if the first rotor is lost. Notice that similar results can be obtained if one of the other actuators is in fault (see equations (28) and (30)). Indeed, if for example motor 2 fails, the third equation of (30) leads to $\bar{u}_5 = 0$ and equations (28) give $v_3(t) = -u_5(t) \leq 0$. Thus, the faulty multirotor turns out to be non reconfigurable.

5.2 Configuration H_2

The H_2 configuration has been studied along similar lines. The mixer matrix is given by equation (19). After multiplication by matrix J^{-1} (equation (13)) and change of variables we get

$$B_{H_2} = \begin{bmatrix} -K_z & -K_z & -K_z & -K_z & -K_z & -K_z \\ -K_r a & -K_r a & -K_r a & K_r a & K_r a & K_r a \\ K_p b & 0 & -K_p b & -K_p b & 0 & K_p b \\ -K_y & K_y & K_y & -K_y & K_y & -K_y \end{bmatrix}. \tag{33}$$

Computing the reduced virtual matrix $B^v{}_{H_2}$ (see (36)) (as for the H_1 configuration), the virtual inputs $\delta v_i(t)$ are given by equations (34):

$$\begin{cases} \delta v_1(t) = \sum_{i=1}^{6} \delta u_i(t) \\ v_2(t) = -2u_1(t) + 2u_5(t) \\ v_3(t) = u_1(t) - u_3(t) - u_4(t) + u_6(t) \\ v_4(t) = u_2(t) - 2u_4(t) + u_5(t) \end{cases} \tag{34}$$

while in hover:

$$\begin{cases} \bar{v}_1 = \sum_{i=1}^{6} \bar{u}_i = \frac{mg}{K_T} \\ \bar{v}_2 = -2\bar{u}_1 + 2\bar{u}_5 = 0 \\ \bar{v}_3 = \bar{u}_1 - \bar{u}_3 - \bar{u}_4 + \bar{u}_6 = 0 \\ \bar{v}_4 = \bar{u}_2 - 2\bar{u}_4 + \bar{u}_5 = 0 \end{cases} \tag{35}$$

$$B^v{}_{H_2} = \begin{bmatrix} -K_z & 0 & 0 & 0 \\ 0 & K_r a & K_r a & -K_r a \\ 0 & 0 & K_p b & 0 \\ 0 & K_y & -K_y & K_y \end{bmatrix}. \tag{36}$$

The system reconfigurability analysis is applied to the faulty multirotor with $u_1(t) = 0$, $\bar{u}_1 = 0$. Then according to equation (35) the loss of motor 1 implies that motor 5 needs to be turned off at least in the equilibrium point. While around the equilibrium the virtual input $v_2(t)$ becomes constrained by zero on one side. Then:

$$\begin{cases} \bar{v}_2 = 2\bar{u}_5 = 0 \\ v_2(t) = +u_5(t) \geq 0. \end{cases} \tag{37}$$

Instead, if only the second rotor is damaged ($u_2(t) = 0$, $\bar{u_2} = 0$) the result is given by equation (38):

$$\begin{cases} \bar{v}_4 = -2\bar{u}_4 + \bar{u}_5 = 0 \\ v_4(t) = -2u_4(t) + u_5(t). \end{cases} \tag{38}$$

Since the faulty rotor does not bring any other rotor to zero, the system turns out to be reconfigurable. Table 1 summarises the results of the reconfigurability analysis applied to H_1 and H_2 if one at a time the rotor speed $u_j(t)$ is set to zero for $j = 1, ..., 6$.

	Reconfigurability
H_1	no reconfigurable
H_2	rotors: 2, 3, 6

Table 1. Summary table of reconfigurable rotors for H_1 and H_2

Note that the propellers direction of rotation influences the system reconfigurability.

5.3 Simulation results

In FTC a diagnosis unit is able to isolate and detect the fault. In this case it is assumed that the fault detection has been already accomplished. Therefore, the diagnoser output is a vector η:

$$\eta = \begin{bmatrix} \eta_1 & \eta_2 & \dots & \eta_{N_r} \end{bmatrix} \tag{39}$$

where N_r corresponds to the number of motor of the multicopter. Each element of η can be 0 (if the corresponding motor failed) or 1 (if the corresponding motor is not in fault). The information given by η is then translated on the input matrix of the system as:

$$B_{H_\eta} = B_H \, diag \begin{bmatrix} \eta_1 & \eta_2 & \dots & \eta_{N_r} \end{bmatrix}. \tag{40}$$

Then the LVA is computed according to equation (5) and applied to the faulty system. The Simulink implementation of the LVA on the multicopter simulator has been performed as depicted in the block diagram in Figure 5.

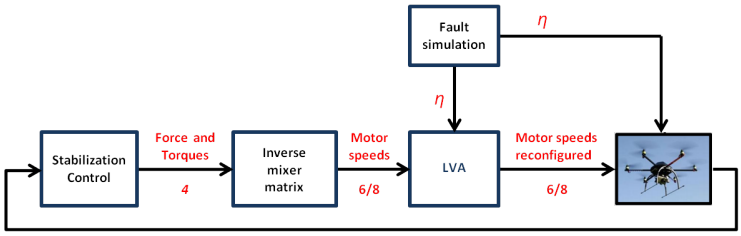

Fig. 5. Reconfiguration block-scheme

A smooth fixed-point trajectory with the multirotor hovering at an altitude of 2.5 m has been considered and the fault has been reproduced, setting to zero at instant $t_f = 20\,s$ one of the motors speed. The reconfiguration occurs at instant $t_r = 20.1\,s$. The time delay $t_r - t_f = 0.1\,s$ has been chosen to be equal to ten times the time cycle of the Flight Control Unit. Even if for each of the configurations taken into account the connection between simulation results and theoretical ones was checked (performing a simulation for each one of the six possible fault occurences), in this work only the response of the system to one faulty case will be shown.

5.3.1 H_1 configuration

Considering the hexacopter H_1 (see Figure 2a) it has been demonstrated that it is not reconfigurable. Then, if the first motor is in fault $u_1(t) = 0$ the result of the simulation is depicted in Figure 6.

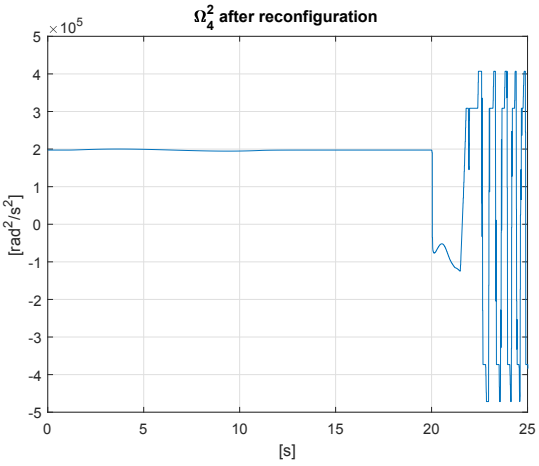

Fig. 6. Rotational speed of rotor number 4.

The LVA tries to bring to zero the speed of the fourth rotor. But before this happens the hexarotor deflects into an area where u_4 should develop a negative speed (see Figure 6) in order to compensate the loss of the first motor. Since this cannot happen the multirotor becomes unstable and falls.

5.3.2 H_2 configuration

In order to show the difference with respect to the previous case, the hexacopter H_2 (see Figure 2b) is considered. Furthermore, it is assumed that u_2 is lost and the control allocator acts 0.1 s after the time instant $t_f = 20$ at which the fault occurs. In order to center the focus on the capability of the system to recover the reference trajectory, only the plots relative to position, attitude and throttles are shown. The results are given by Figures 7, 8 and 9.

Notice that, according to theory the multicopter is reconfigurable with respect to a fault on the second rotor. Indeed the LVA manages to reconfigure the speeds of each rotor in order to bring the aircraft in hovering condition. Furthermore, the greatest value of throttle is given by motor three, which is on the same axis of the faulty engine and rotates in the same direction. This consideration justifies the fact that it has to develop more torque with respect to the other rotors.

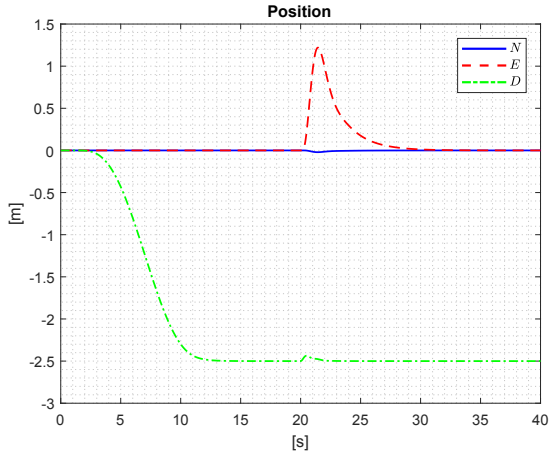

Fig. 7. H_2: Position response

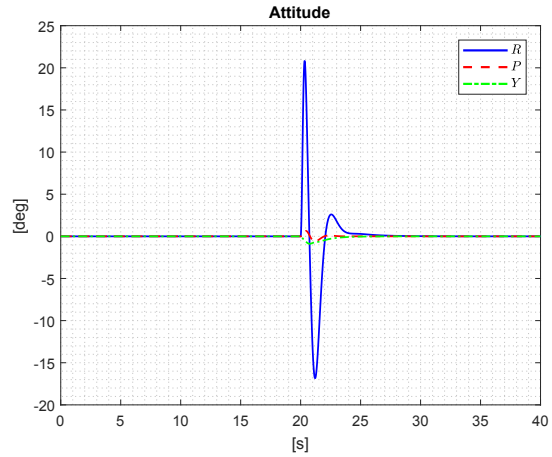

Fig. 8. H_2: Attitude response.

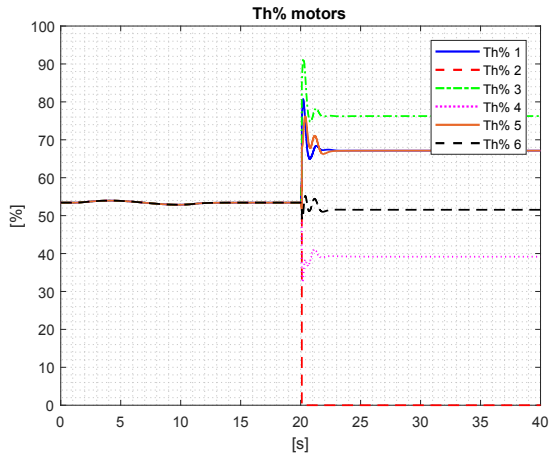

Fig. 9. H_2: Throttles reconfigured

6 Octocopter

Applying the same reconfigurability analysis to matrices (20) and (21) of the octocopters O_1 and O_2 respectively, the following equations and matrices are obtained for O_1:

$$B^v{}_{O_1} = \begin{bmatrix} -K_z & 0 & 0 & 0 \\ 0 & -K_r a_{\frac{3\pi}{8}} & -K_r a_{\frac{\pi}{8}} & -K_r a_{\frac{\pi}{8}} \\ 0 & K_p b_{\frac{3\pi}{8}} & K_p b_{\frac{3\pi}{8}} & -K_p b_{\frac{\pi}{8}} \\ 0 & K_y & -K_y & K_y \end{bmatrix} \tag{41}$$

$$\begin{cases} \delta v_1(t) = \sum_{i=1}^{8} \delta u_i(t) \\ v_2(t) = u_1(t) - u_4(t) - (\sqrt{2}-1)u_5(t) - (2-\sqrt{2})u_6(t) + (2-\sqrt{2})u_7(t) + (\sqrt{2}-1)u_8(t) \\ v_3(t) = u_2(t) + (\sqrt{2}-1)u_4(t) - 2(\sqrt{2}-1)u_5(t) - (3-2\sqrt{2})u_6(t) - 2(\sqrt{2}-1)u_7(t) + ... \\ ... + (\sqrt{2}-1)u_8(t) \\ v_4(t) = u_3(t) + (\sqrt{2}-1)u_4(t) + (2-\sqrt{2})u_5(t) - (2-\sqrt{2})u_6(t) - (\sqrt{2}-1)u_7(t) - u_8(t) \end{cases} \tag{42}$$

and for O_2:

$$B^v{}_{O_2} = \begin{bmatrix} -K_z & 0 & 0 & 0 \\ 0 & -K_r a_{\frac{3\pi}{8}} & -K_r a_{\frac{\pi}{8}} & -K_r a_{\frac{\pi}{8}} \\ 0 & K_p b_{\frac{3\pi}{8}} & K_p b_{\frac{3\pi}{8}} & -K_p b_{\frac{\pi}{8}} \\ 0 & K_y & K_y & -K_y \end{bmatrix} \tag{43}$$

$$\begin{cases} \delta v_1(t) = \sum_{i=1}^{8} \delta u_i(t) \\ v_2(t) = u_1(t) - u_4(t) - (\sqrt{2}+1)u_5(t) - (\sqrt{2})u_6(t) + (\sqrt{2})u_7(t) + (\sqrt{2}+1)u_8(t) \\ v_3(t) = u_2(t) + (\sqrt{2}-1)u_4(t) + 2u_5(t) + u_6(t) - 2u_7(t) - (\sqrt{2}+1)u_8(t) \\ v_4(t) = u_3(t) + (\sqrt{2}-1)u_4(t) - \sqrt{2}u_5(t) - \sqrt{2}u_6(t) + (\sqrt{2}-1)u_7(t) + u_8(t). \end{cases} \tag{44}$$

In order to test the reconfigurability of O_1, it is supposed that motor 1 fails. Equations (42), in hover, become:

$$\begin{cases} \bar{v}_1 = \sum_{i=2}^{8} \bar{u}_i = \frac{mg}{K_T} \\ \bar{v}_2 = -\bar{u}_4 - (\sqrt{2}-1)\bar{u}_5 - (2-\sqrt{2})\bar{u}_6 + (2-\sqrt{2})\bar{u}_7 + (\sqrt{2}-1)\bar{u}_8 = 0 \\ \bar{v}_3 = \bar{u}_2 + (\sqrt{2}-1)\bar{u}_4 - 2(\sqrt{2}-1)\bar{u}_5 + (3-2\sqrt{2})\bar{u}_6 - (2\sqrt{2}-1)\bar{u}_7 + (\sqrt{2}-1)\bar{u}_8 = 0 \\ \bar{v}_4 = \bar{u}_3 + (\sqrt{2}-1)\bar{u}_4 + (2-\sqrt{2})\bar{u}_5 - (2-\sqrt{2})\bar{u}_6 - (\sqrt{2}-1)\bar{u}_7 - \bar{u}_8 = 0. \end{cases} \tag{45}$$

Notice that condition $\bar{u}_1 = 0$ does not force any other rotor to zero. Furthemore, there does not exist any faulty virtual input $\delta v_i(t)$ which contains the fault ($u_1(t)$) and that becomes constrained on one side by zero. In fact, $v_2(t)$ (equation (46)) after the fault continues to be either positive or negative.

$$\begin{cases} \delta v_1(t) = \sum_{i=2}^{8} \delta u_i(t) \\ v_2(t) = u_1(t) - u_4(t) - (\sqrt{2}-1)u_5(t) - (2-\sqrt{2})u_6(t) + (2-\sqrt{2})u_7(t) + (\sqrt{2}-1)u_8(t) \\ v_3(t) = u_2 + (\sqrt{2}-1)u_4(t) - 2(\sqrt{2}-1)u_5(t) + (3-2\sqrt{2})u_6(t) - (2\sqrt{2}-1)u_7(t) + \\ \ldots + (\sqrt{2}-1)u_8(t) \\ v_4(t) = u_3(t) + (\sqrt{2}-1)u_4(t) + (2-\sqrt{2})u_5(t) - (2-\sqrt{2})u_6(t) - (\sqrt{2}-1)u_7(t) - u_8(t) \end{cases} \tag{46}$$

The same conclusion is reached in the case of loss of any of the other motors. Therefore, the octocopter O_1 is fully reconfigurable against the loss of any one of its motors.

Focusing on O_2 and supposing that motor 1 is lost, we get

$$\begin{cases} \bar{v}_1 = \sum_{i=2}^{8} \bar{u}_i = \frac{mg}{K_T} \\ \bar{v}_2 = -\bar{u}_4 - (\sqrt{2}+1)\bar{u}_5 - (\sqrt{2})\bar{u}_6 + (\sqrt{2})\bar{u}_7 + (\sqrt{2}+1)\bar{u}_8 = 0 \\ \bar{v}_3 = \bar{u}_2 + (\sqrt{2}-1)\bar{u}_4 + 2\bar{u}_5 + \bar{u}_6 - 2\bar{u}_7 - (\sqrt{2}+1)\bar{u}_8 = 0 \\ \bar{v}_4 = \bar{u}_3 + (\sqrt{2}-1)\bar{u}_4 - \sqrt{2}\bar{u}_5 - \sqrt{2}\bar{u}_6 + (\sqrt{2}-1)\bar{u}_7 + \bar{u}_8 = 0 \end{cases} \tag{47}$$

$$\begin{cases} \delta v_1(t) = \sum_{i=2}^{8} \delta u_i(t) \\ v_2(t) = -u_4(t) - (\sqrt{2}+1)u_5(t) - (\sqrt{2})u_6(t) + (\sqrt{2})u_7(t) + (\sqrt{2}+1)u_8(t) \\ v_3(t) = u_2(t) + (\sqrt{2}-1)u_4(t) + 2u_5(t) + u_6(t) - 2u_7(t) - (\sqrt{2}+1)u_8(t) \\ v_4(t) = u_3(t) + (\sqrt{2}-1)u_4(t) - \sqrt{2}u_5(t) - \sqrt{2}u_6(t) + (\sqrt{2}-1)u_7(t) + u_8(t). \end{cases} \tag{48}$$

According to equations (48), $\delta v_1(t)$ and $v_2(t)$ can be positive or negative after the loss of motor 1. Note that, testing the other motors the outcome does not change. Then, also the octocopter O_2 is fully reconfigurable.

6.1 Simulation results

The implementation of the LVA on the multicopter simulator follows the strategy presented in Figure 5. Also in this case, the pertinence of theoretical and simulation results has been verified for each motor and in both the multirotor configurations. Both octocopter configurations (see Figures 3b and 3a) are fully reconfigurable; thus, the two multirotors are compared in the case $u_1(t)$ fails. In order to center the focus on the capability of the system to recover the hovering reference, only the plots relative to position, attitude and throttles are presented. The results of the simulations are given in Figures 10, 11 and 12 for O_1, while in Figures 13, 14 and 15 for O_2.

The two multirotors are reconfigurable with respect to a fault on $u_1(t)$, but while the maximum throttle developed in O_2 (see Figure 15) is generated by the second motor, in O_1 it is given by motors 3 and 7 (see Figure 12). Therefore, in the recon-

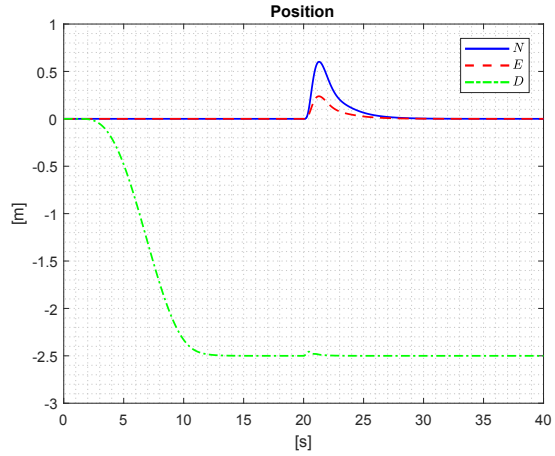

Fig. 10. O_1: Position response

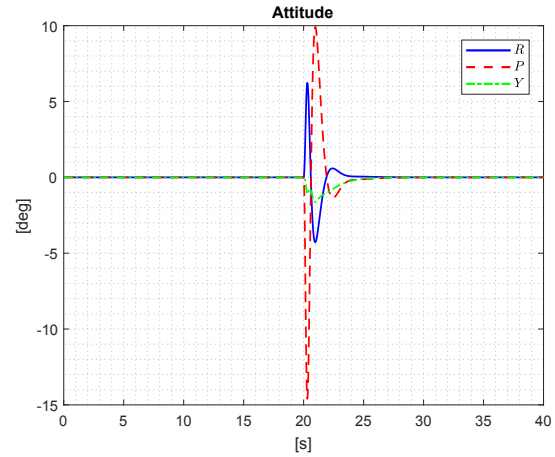

Fig. 11. O_1: Attitude response

figured octocopter O_1 the throttles are better redistributed with respect to O_2. Notice also that the maximum peak of the throttles in O_1 is smaller respect to O_2.

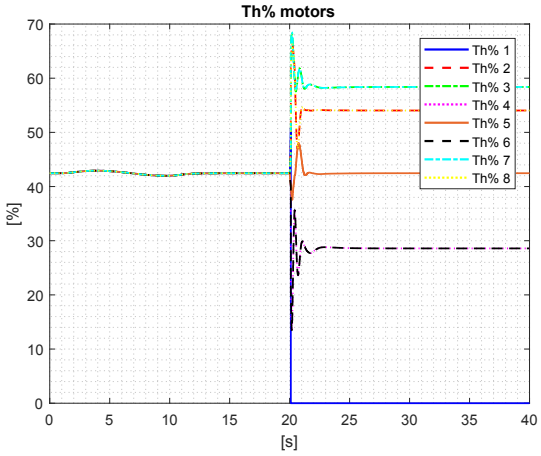

Fig. 12. O_1: Throttles

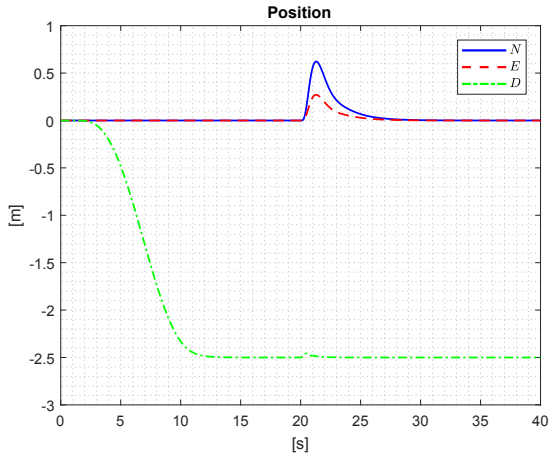

Fig. 13. O_2: Position response

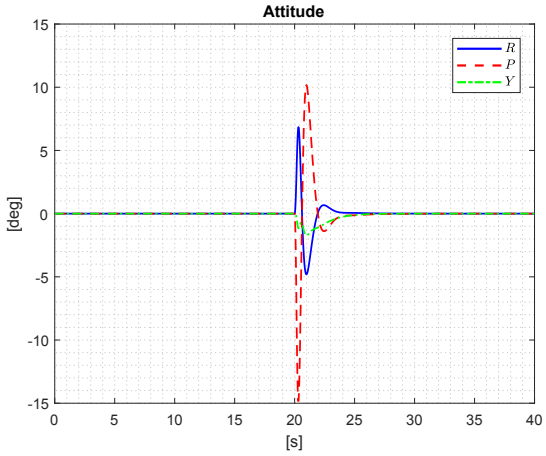

Fig. 14. O_2: Attitude response

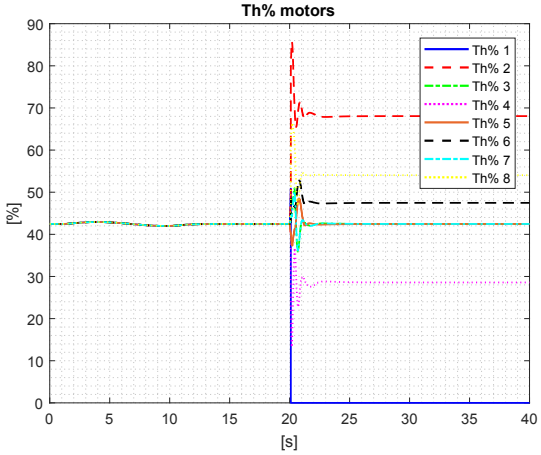

Fig. 15. O_2: Throttles

7 Conclusion

The problem of reconfigurability analysis for multirotor UAVs has been considered. The method proposed in[1] has been used and four configurations, two hexacopters with H geometry and two octocopters have been analysed. Simulation results are used to validate the conclusions of the analysis and to study the sensitivity of the actual reconfiguration to the detection delay.

References

[1] D. Vey and J. Lunze. Structural reconfigurability analysis of multirotor uavs after actuator failures. In *IEEE Conference on Decision and Control (CDC)*. IEEE, 2015.

[2] G.-X. Du, Q. Quan, B. Yang, and K.-Y. Cai. Controllability Analysis for Multirotor Helicopter Rotor Degradation and Failure. *Journal of Guidance, Control and Dynamics*, 38(5):978–985, 2015.

[3] M. Bergamasco and M. Lovera. Identification of linear models for the dynamics of a hovering quadrotor. *IEEE Transactions on Control Systems Technology*, 2014.